Facile Synthesis of Nanostructured Carbon through Self-Assembly between Block Copolymers and Carbohydrates

ARTICLE *in* ADVANCED FUNCTIONAL MATERIALS · AUGUST 2007

Impact Factor: 11.81 · DOI: 10.1002/adfm.200600952

FULL PAPER

ADVANCED FUNCTIONAL MATERIALS

DOI: 10.1002/adfm.200600952

Facile Synthesis of Nanostructured Carbon through Self-Assembly between Block Copolymers and Carbohydrates**

By *Adrian T. Rodriguez*, *Xuefa Li*, *Jin Wang*, *William A. Steen*, and *Hongyou Fan**

A simple and direct wet chemistry method is reported to simultaneously synthesize nanostructured carbon films and particles through self-assembly of poly(styrene)-poly(4-vinylpyridine) (PS-P4VP) and carbohydrate precursors (turanose, raffinose, glucose, etc.) in two fabrication processes—spin-coating and aerosol processing. Starting with a homogeneous solution containing PS-P4VP and carbohydrates, evaporation of solvent during either spin-coating or an aerosol process leads to the formation of ordered mesostructured films and particles. High temperature treatment in argon atmosphere removes PS fragments, carbonizes carbohydrates and partial PVP fragments, and results in ordered nanoporous carbon films and particles. SEM, TEM, and GISAXS characterization indicates that these nanostructured carbon materials exhibit large nanopores (>20 nm), controlled 1–3 dimensional structures, and controlled surface chemistry. Nitrogen sorption isotherms and electrochemistry characterization indicates the accessibility of the carbon nanopores to both gas phase and aqueous phase. Results suggest that the nanostructured carbon films and particles can be tuned through solvent annealing, precursor concentration, and choice of block copolymers used. These carbon materials present varied practical applications for sorption and separation, sensors, electrode materials, etc.

1. Introduction

Nanostructured carbon materials, including carbon nanotubes,[1,2] membranes,[3] and particles,[4–7] are an important nanomaterial for many applications in nanoelectronics,[8] sorption and separation,[3] sensors,[9] catalysis,[7] and energy conversion and storage (e.g., double layer capacitors,[10] and hydrogen storage[11]). Varied methods have been developed to synthesize nanostructured carbon materials, such as DC arc-discharge, laser ablation, chemical vapor deposition,[2] templating,[6,12–19] etc. However, direct fabrication of complex carbon nanostructures with controlled form (e.g., film, particle, tube, etc.), dimension, and surface architecture remains a significant challenge. Recently we developed a simple and direct synthetic method to prepare nanoporous carbon nanotubes with large pores (>20 nm) on the tube wall.[20] The method involved coating of porous anodic aluminum oxide (AAO) inner pore channel surface with block copolymer (polystyrene-*co*-poly(vinylpyridine)) and carbohydrates in DMF solution. Drying of DMF induced micro-phase separation of PS-PVP and formation of ordered PS and PVP/carbohydrate domains. Within the coating, the carbohydrates stay specifically only in the pyridine domains surrounding PS domains due to the interaction between carbohydrates and pyridine blocks. After carbonization at high temperature in argon, PS fragments were removed, forming the nanopores and carbohydrates were carbonized, forming the framework of nanoporous carbon tubes within AAO channels. Removal of AAO leads to the formation of individual monodisperse nanoporous carbon nanotubes with tube wall of ~16 nm. Here, we extend this method by combining self-assembly of polymer and carbohydrates with two fabrication procedures—spin-coating and aerosol processing—to form nanostructured carbon films and particles with controlled 1–3 dimensional features. The formation of these nanostructured carbon materials was driven by the interaction between polystyrene-*co*-poly(4-vinylpyridine) (PS-P4VP) and environmentally benign carbohydrate precursors during phase separation that occurs in both fabrication processes. Subsequent high

[*] Prof. H. Fan, Dr. W. Steen
Sandia National Laboratories, Advanced Materials Laboratory
1001 University Blvd. SE, Albuquerque, NM 87106 (USA)
E-mail: hfan@sandia.gov
Prof. H. Fan, A. Rodriguez
Department of Chemical and Nuclear Engineering
NSF Center for Micro-Engineered Materials
University of New Mexico
Albuquerque, NM 87131 (USA)
Dr. X. F. Li, Dr. J. Wang
Argonne National Laboratory Advanced Photon Source
Argonne, IL 60439 (USA)

[**] We thank Darren Dunphy, Eric Branson, Adam Cook, and Deanna Lopez for their assistance on GISXAS experiments and Zhu Chen for his assistance on FTIR studies. This work was partially supported by the U.S. Department of Energy (DOE) Basic Energy Sciences Program, Sandia National Laboratory's Laboratory Directed R&D program, and Center for Integrated Nanotechnologies (CINT). TEM studies were performed in the Department of Earth and Planetary at University of New Mexico. We acknowledge the use of the SEM facility supported by the NSF EPSCOR and NNIN grants. The authors also would like to acknowledge the staff support at the APS and the use of APS 8-ID-E beamline facility that is supported by the Department of Energy under contract W-31-109-ENG-38. Sandia is a multiprogram laboratory operated by Sandia Corporation, a Lockheed Martin Company, for the United States Department of Energy's National Nuclear Security Administration under Contract DE-AC04-94AL85000. Supporting Information is available online from Wiley InterScience or from the authors.

ADVANCED FUNCTIONAL MATERIALS

temperature carbonization of the carbohydrate/polymer composite in an argon environment leads to ordered and nanoporous carbon materials. The ease with which these carbon materials can be fabricated, and the ability to tune forms, nanostructures, and surface chemistry through the choice of synthesis procedures, block copolymers used, and carbonization temperature, should facilitate investigations of varied practical applications for sorption and separation, sensors, electrode materials, etc.

Using a self-assembling solution, we developed a simple and direct wet chemistry method to simultaneously synthesize nanoporous carbon films and particles by combining hydrogen bonding assisted self-assembly of PS-P4VP and carbohydrate precursors with two fabrication processes—spin-coating[21] and aerosol processing.[22] These nanostructured carbon materials exhibit large nanopore (>20 nm), controlled 1–3 dimensional structures, and surface chemistry. Scheme 1 illustrates the hydrogen bonding driven self-assembly of carbohydrates and PS-P4VP and the formation of ordered, nanoporous carbon materials. Carbohydrates (such as turanose, raffinose, sucrose, etc.) are environmentally benign and often used as precursors to synthesize carbon materials.[4,6] Under mild temperature (140–180 °C), incomplete carbonization led to formation of carboneous materials containing aromatic benzene rings and hydroxyl groups.[5] Complete carbonization occurs at higher temperature (>400 °C).[4] To facilitate self-assembly and formation of ordered nanoporous carbon materials, we chose PS-PVP block copolymers where the PVP block has equal or larger fragment sizes than PS in order to form a PS core surrounded by PVP during micro-phase separation. Addition of carbohydrates and their subsequent self-assembly with PVP fragments further increases the volume fraction of polar species (PVP + carbohydrates), ensuring the PS core and PVP/carbohydrate shell structure. Thus, ordered PS-PVP/carbohydrates nanocomposite films are finally formed. After treatment at high temperature (>460 °C) in argon, the PS fragments were removed, forming the mesopore; carbohydrates/PVP were carbonized, forming the framework of nanoporous carbon films and particles.

2. Results and Discussion

Our carbon nanostructure preparation process begins with a homogenous self-assembling solution containing block copolymers and carbon precursors. In a typical preparation (see Experimental Sec. for more details), carbohydrate precursors such as turanose, raffinose, glucose, etc. were added to dimethyl formamide (DMF) for sonication. Before the addition of PS-P4VP, the carbohydrates precursors were hardly soluble in DMF at room temperature, even under the assistance of sonication. After the addition of PS-P4VP, the carbohydrate precursors quickly dissolved in DMF. We believe that this is caused by the formation of hydrogen bonds between the carbohydrates and pyridine blocks, which promotes the dissolution of carbohydrate precursors in DMF. Hydrogen bonds formation has been investigated and confirmed by FTIR studies. Figure 1 shows FTIR spectra of pure PS-P4VP, carbohydrate/PS-P4VP films spin-coated by using a self-assembly solution with and without heat treatment at 180 °C for three hours. According to previous FTIR studies, formation of hydrogen bonds between PVP and hydroxyl groups causes changes of the electronic distributions in the pyridine ring resulting in shifts for the stretching modes of the pyridine ring.[23–25] In comparison with the spectra of pure PS-P4VP, the PVP characteristic peaks at 1597, 1415, and 993 cm^{-1} have shifted, suggesting the formation of hydrogen bonds between the hydroxyl groups of the carbohydrates and nitrogen groups of the pyridines. In both heated and unheated solutions, these shifts were observed. The results also indicated that the samples that were heated at 180 °C showed more shifts than the unheated solutions. This may suggest that heat treatment is favourable for the hydrogen bonding and self-assembly process. The hydrogen bonding behaviour has been observed in other carbon precursors and polymer systems.[19,26] The new peaks appeared between 1000–1300 cm^{-1} after heat-treatment, suggesting that Maillard reactions between the pyridine blocks and carbohydrates may occur. This could be another reason that the carbohydrates remain exclusively in PVP domains, enhancing the self-assembly process. Further detailed studies of these reactions were in progress.

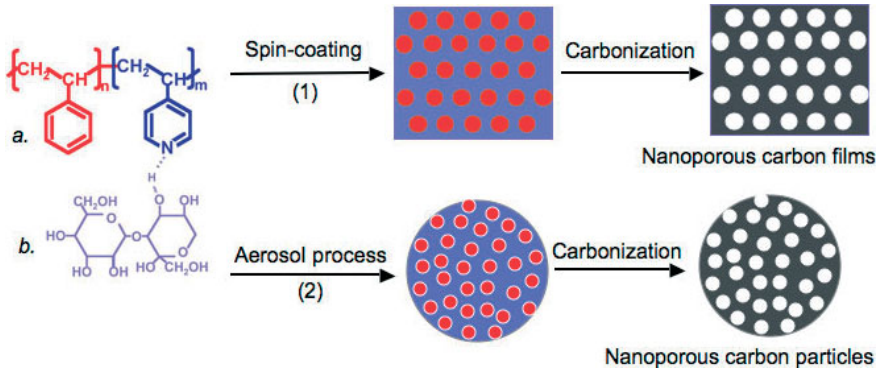

Scheme 1. Formation of nanostructured carbon materials through hydrogen bonding assisted self-assembly of *a*, poly(styrene)-poly(4-vinylpyridine) (PS-P4VP) and *b*, environmentally benign carbohydrates (e.g., sucrose, turanose, raffinose etc.) in two self-assembly processes. 1) Ordered nanoporous carbon films were deposited on substrates (such as silicon wafer, glass slides, gold electrodes, and other patterned surfaces) through spin-coating. 2) Spherical nanoporous carbon particles were synthesized through an aerosol-assisted self-assembly process.

Nanostructured carbon films were deposited on (100)-silicon by spin-coating at 500–2000 rpm for two minutes. During spin-coating, evaporation of DMF progressively enriches the concentrations of the non-volatile constituents including carbohydrates and PS-P4VP on the substrates. Drying induces microphase separation and formation of ordered PS-

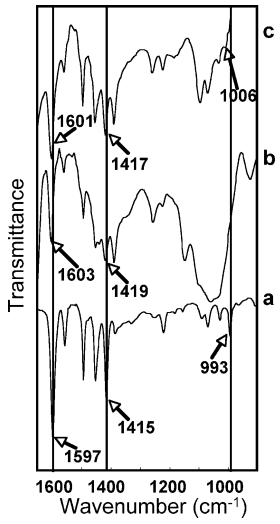

Figure 1. FTIR spectra of a) pure PS-P4VP (polymer source, $M_n^{PS} = 12\,000$ g mol^{-1}, $M_n^{PVP} = 11\,800$ g mol^{-1}, with molecular size distribution of 1.04), carbohydrates/PS-P4VP films spin-coated by using solution with (b) and without (c) without heat treatment at 180 °C for three hours.

P4VP/carbodryates composite films. The hydrogen bonding between carbohydrates and PVP blocks retains carbohydrates exclusively in PVP phase, surrounding PS phase (see Scheme 1, process 1). After annealing in DMF/benzene vapor at 80 °C overnight, the final films were carbonized at higher temperatures to produce 3-dimensional nanoporous carbon films. According to the thermogravimetric studies (Supporting Information Fig. S1), significant weight loss of ~64 % occurred from 200 °C to 450 °C, which are mainly attributed to the decomposition of turanose and some of PS-P4VP. Weight loss before 200 °C are attributed to solvents. These results suggest a minimum temperature to remove PS-P4VP and to carbonize turanose, creating pore structure at ~450 °C. In this temperature window, two losses were observed, which were attributed to the carbonization of turanose and polymer. Based on TGA curves at 600 °C, ~40 % of carbon was from PVP and ~60 % was from turanose.

The nature of the carbon framework has been studied using FTIR, ^{13}C-NMR, and wide-angle XRD. FTIR spectra performed on the carbonized films revealed the existence of hydroxyl bands at the range of 3400–3700 cm^{-1} (Supporting Information Fig. S2). Observed peaks at 3425, 3555, and 3633 cm^{-1} correspond to the stretching band of hydrogen bonded and free—OH groups on an aromatic ring, respectively. The –OH groups can be potentially used for further pore surface functionalization through a variety of siloxane chemistries.[21] What's more, the high polarity of –OH groups could potentially lead to fast and strong absorption and chemical selectivity for sensors and/or purification and separation.[27] The peak at 3058 cm^{-1} and 1600 cm^{-1} corresponds to the =C–H stretch and C=C of a benzene ring, respectively. The single resonance at $\delta = 110.6$ ppm (Supporting Information Fig. S3) suggests the existence of sp^2 carbon species, which is consistent with FTIR results. Wide-angle XRD (Supporting Information Fig. S4) shows a broad peak at ~40 °, suggesting an amorphous carbon nature rather than graphitic structure. These results establish the final material framework to be non-graphitic carbon materials.[28]

Representative plan-view scanning electron microscopy (SEM) images of nanoporous carbon films are shown in Figure 2a and b. The film is macroscopically smooth and free of cracking. The films have large areas of regular in-plane hexagonal pore structure with the spatial period of ~28 nm. The cell

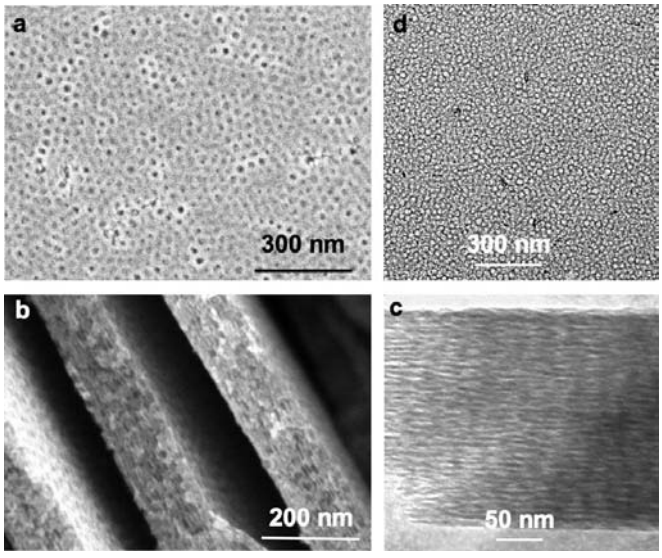

Figure 2. Representative plan-view and cross-sectional view scanning electron microscopy (SEM, a and b) and transmission electron microscopy (TEM, c and d) images of 3-dimensional mesoporous carbon films. Image b shows cross-sectional view of three individual films. These films were prepared by using a homogenous DMF solution containing 8.7 wt % turanose and 4.3 wt % PS-P4VP (polymer source, $M_n^{PVP} = 12\,000$ g mol^{-1}, $M_n^{PVP} = 11\,800$ g mol^{-1}, with molecular size distribution of 1.04). The precursor solutions were heated at 180 °C for 3 h before spin-coating. After spin-coating, all films were annealed at 80 °C for 1 day in DMF and benzene vapor. The films were carbonized at 600 °C for 1 h in argon.

parameter estimated from the high resolution SEM (Fig. 2) is approximately 20 nm, which is consistent with the value determined from the GISAXS data (see below). The cell size and pore wall can be controlled by the domain size of PS and the volume fraction of added carbohydrates. By increasing the amount of carbohydrates in the initial coating solution, the pore-to-pore distance in the final nanoporous carbon film increases (Supporting Information Fig. S5), which suggests that the pore wall thickness increases. Figure 2d shows representative cross-sectional SEM image of nanoporous carbon film with thickness of ~100 nm. The film has an undulated lamellar structure throughout the entire film thickness. The interlayer *d*-spacing is between 4–6 nm which is further confirmed by GISAXS studies (see below). Figure 2c shows a representative plan-view TEM image that shows the film is uniform and has local hexagonal arrays. The average cell size measured from TEM image is approximately 21 nm. No graphitic microstruc-

ADVANCED FUNCTIONAL MATERIALS

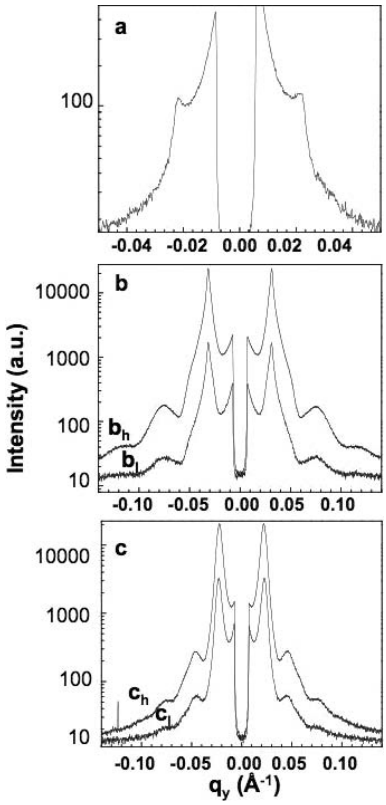

Figure 3. GISAXS linescans: a) pure PS-P4VP, b) as-prepared film, and c) after anneal at 80 °C overnight. b_h and c_h are high angle GISAXS data, b_l and c_l are low angle GISAXS data. Sample b and c were prepared by using a homogenous DMF solution containing 8.7 wt % turanose and 4.3 wt % PS-P4VP (polymer source, M_n^{PS} = 12 000 g mol^{-1}, M_n^{PVP} = 11 800 g mol^{-1}, with molecular size distribution of 1.04) (see Experimental section).

ture was observed in the high resolution TEM images, which suggests that the pore wall is amorphous carbon. The cross-sectional TEM image in Figure 2d shows undulated laminated structure with interlay *d*-spacing of 4–8 nm. Both SEM and TEM results confirm that the nanoporous carbon films exhibit 3-dimensional perforated lamellar pore structure.[29]

To better understand the self-assembly process and formation of ordered 3-dimensional porous carbon nanostructure, we carried out GISAXS studies. We first studied the self-assembly behaviour of PS-P4VP before and after addition of carbohydrates. GISAXS data for pure PS-P4VP films show only one order of in-plane (*x* and *y*) scattering pattern at 23 nm (Fig. 3a), a reflection of characteristic polymer micellar structure. The average separation distance between each domain (PS) is 26.5 nm. Addition of carbohydrates induces hydrogen bonding between carbohydrates and PVP blocks and leads to much higher ordered film structure with respect to pure PS-P4VP. GISAXS linescan data (Fig 3b) for the carbohydrate/PS-P4VP film after spin-coating and drying shows two broad peaks readily observable from in-plane diffraction at 20.3 nm, attributed to local hexagonal structure. The average separation distance between each domain (PS) decreases to 23.3 nm. Upon annealing in DMF/Benzene vapor at 80 °C overnight, the lateral/in-plane ordering of the films improves further. Consequently, three orders of the in-plane diffraction peaks are seen (Fig 3c). These orders are sharper than those before the annealing process, corresponding to the (10), (11), and (20) reflections of a 1-dimensional hexagonal lattice with a d_{100}-spacing of 27.3 nm. The GISAXS results further confirm the hydrogen bonding self-assembly process between PS-PVP and carbohydrates, explaining the enhanced solubility of carbohydrates in DMF after addition of PS-PVP block copolymers, and support the conclusion from FTIR studies.

Figure 4 shows the GISAXS results of nanoporous carbon films. The X-ray penetration depth can be controlled by the incident angle, providing details on the depth dependence of the thin-film structure. A critical angle, α, was first determined by

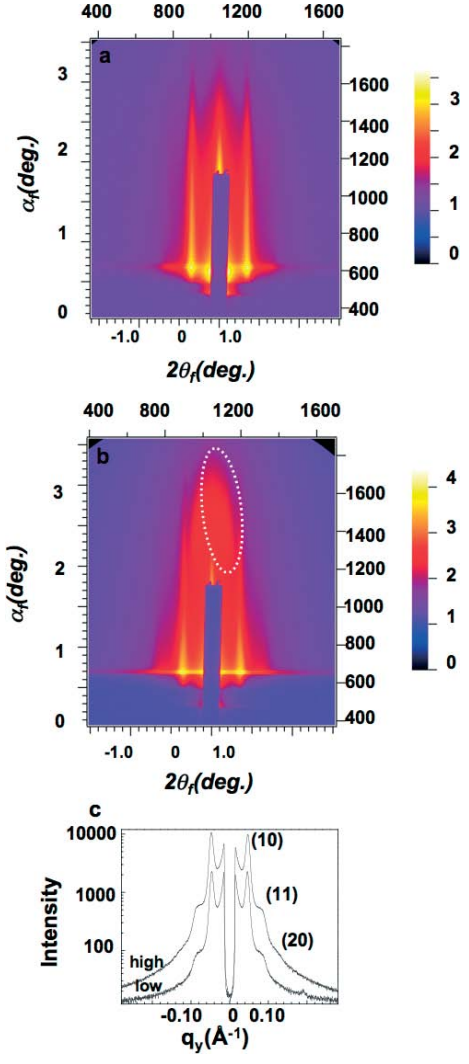

Figure 4. Grazing incidence small-angle X-ray scattering (GISAXS) characterization of 3D nanoporous carbon films. Sample was prepared by using a homogenous DMF solution containing 8.7 wt % turanose and 4.3 wt % PS-P4VP (polymer source, M_n^{PS} = 12 000 g mol^{-1}, M_n^{PVP} = 11 800 g mol^{-1}, with molecular size distribution of 1.04), carbonized at 600 °C in argon for 1 h. a) Data acquired at lower than the critical angle. b) Data acquired at higher than critical angle with full film penetration, showing ordered features from both *xy*- and *z*-directions (*z*-direction indicated as the dot circle). *c*, q_y linescans. The carbon film sample shows consistent hexagonal structures throughout the film thickness.

reflectivity scans. A series of incident angles were then used to achieve penetration depths from several angstroms to full penetration into the film. Below *a*, as shown in Figure 4a, the (10) and (11) scattering peaks of hexagonal arrays are clearly observable. As shown in Figure 4b, this in-plane order was maintained when the incident angle is above a, suggesting a consistent, ordered pore structure through the whole film thickness. In addition to (10) and (11) peaks, a third peak appeared and can be indexed as (21). Based on hexagonal symmetry, the calculated unit cell $a = \sim 27.1$ nm. In the z-direction (vertical to film/substrate), the carbon films show one scattering peak attributed to a lamellar mesostructure with an average interlayer spacing of approximately 5 nm. The GISAXS data further confirms the 3-dimensional perforated lamellar pore structure that been observed in SEM and TEM images.

The microstructures of block copolymer films were very sensitive to different solvent vapors and dependent on each block fraction. We were able to tune the film microstructure by annealing as-prepared carbohydrate/PS-PVP films in different solvent vapors and changing fragment volume fraction. After spin-coating and drying, we annealed the PS-P4VP/carbohydrate films in different solvents such as DMF, benzene, THF, DMOS, and water at 80 °C. We found that DMF/benzene was the best solvent pair in refining the ordering of PS-P4VP/carbohydrate films and facilitating the formation of ordered nanoporous carbon films. In addition to 3-dimensional mesostructure, other structures, such as worm-like and foam like structures, were prepared through annealing in different solvent vapors (see Supporting Information Fig. S6). Film nanostructures can be further tuned by using relative weight fractions. We found that when less than 5 wt % of carbohydrates were used, the 3-dimensional perforated lamellar mesophase was obtained in general; increasing carbohydrates to 7 wt % or more, the mesophase changed from 3-dimensional perforated lamellar mesophase to swirling tubular channels (see Supporting Information Fig. S7).

A surface acoustic wave technique was used to determine pore accessibility of the supported films.[30] Nitrogen sorption isotherms of the carbonized films show a type IV curve with a capillary condensation step at $P/P_0 = 0.5$–0.8 and an H_1-type hysteresis loop, suggesting large mesopores (Fig. 5). The BET surface areas, porosity, and average pore size calculated using BJH model are 530 $m^2 g^{-1}$, 40 %, and 16 nm, respectively, demonstrating the accessibility of the mesoporosity to the vapor phase.

To demonstrate that the mesoporosity is accessible to an aqueous phase and to prove viability for future applications, the capacitance of the nanoporous carbon films was probed. Figure 6 shows background subtracted cyclic voltammograms (CVs) at various scan rates in 2 M H_2SO_4. These CVs first prove that the carbon film has sufficient electrical conductivity and adherence to the Au substrate to participate in applicable electrochemical experiments. While these films do not exhibit perfect rectangular CVs (meaning double layer charging/discharging is not instantaneous) and have some pseudo-capacitance (the small peaks ~0.2–0.3 V_{SCE}), the large current confirms electrical double layer capacitance (EDLC) and the current increases with increasing scan rate, as expected. Since capacitance is dq/dE where q is the charge (coulombs) and E is the potential (volts), taking the plateau current and dividing by the respective scan rate should result in capacitance (farads). However, since there is a slight skew to these CVs (especially at higher scan rates), the current was integrated as a function of time and divided by the potential window (0.7 V). This re-

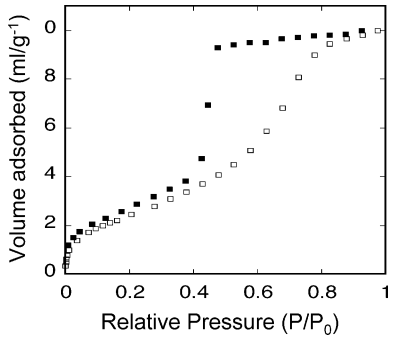

Figure 5. Nitrogen sorption isotherms of 3D nanoporous carbon films prepared by using turanose (7.1 wt %) and 0.1 g wt % PS-P4VP (polymer source, $M_n^{PS} = 12\,000$ g mol^{-1}, $M_n^{PS} = 11\,800$ g mol^{-1} with molecular size distribution of 1.04). The measurement was conducted at 77 k using surface acoustic wave techniques. The film was applied to ~1 cm^2 area of a piezoelectric ST-cut quartz substrate with interdigitated gold transducers designed to operate at ~97 MHz. Mass change was monitored (~80 pg cm^{-2}) as a functional of relative pressure using a surface acoustic wave technique.

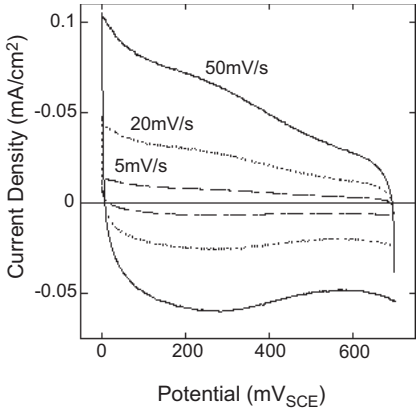

Figure 6. Cyclic voltammograms for a 100 nm thick, 40 % porosity carbon film on gold substrate (current density is normalized per geometric surface area, 1 cm^2). Electrolyte was 2 M H_2SO_4, scan rates were varied as follows: 5 mV s^{-1} (- - -), 20 mV s^{-1} (···), and 50 mV s^{-1} (solid line). The expected rectangular shape is slightly violated at higher scan rates. Resulting specific capacitance is 81.3 F g^{-1} or 14.8 μF cm^{-2} (surface area = 550 $m^2 g^{-1}$), which compares very well to mesoporous carbon powders (~10 μF cm^{-2}). The specific capacitance of the nanoporous carbon films was found using a standard three-electrode arrangement with a BAS 100B potentiostat, a saturated calomel electrode (SCE) reference electrode, and platinum gauze as the counter electrode. A flat cell (PAR KO235) was used which exposes 1 cm^2 of the working electrode. Background cyclic voltammograms (CVs) were first performed on a Au substrate in 2 M H_2SO_4 between 0 and 0.7 V_{SCE} at scan rates varying from 5 to 50 mV s^{-1}. CVs were then performed on a carbon film 100 nm thick with 40 % porosity on a Au substrate.

ADVANCED FUNCTIONAL MATERIALS

sulted in a specific capacitance of (81.3 ± 2.8) F g^{-1}, which compares well to an example mesoporous carbon powder (120 F g^{-1}, 1257 m^2 g^{-1}, pore size 2.3 nm).[10] It is important to note that the nanoporous carbon film has only a fraction of the surface area of the carbon powder, meaning the carbon film has almost 70 % of the specific capacitance of the mesoporous carbon powder while having only 44 % of the surface area. Thus, the carbon film has 50 % more capacitance per unit area (14.8 versus 9.6 μF cm^{-2}) than this example mesoporous carbon,[10,31] which is typical. Because the carbon film does not need binders (which may block the 2.3 nm pores of the powdered carbon) to make a usable electrode, more of the interconnected pores remain undamaged and available for capacitance charging. Furthermore, the carbon film can be fabricated to any shape/form factor and can potentially take advantage of organic electrolytes because of the larger pore size.[32]

By combining the hydrogen bonding assisted self-assembly with an aerosol process[22] (Scheme 1, process 2), we were able to directly synthesize spherical nanostructured carbon particles. Our process started with the identical self-assembling solutions that were used for the synthesis of nanostructured carbon films. Using an aerosol apparatus (Supporting Information Fig. S8), we generated an aerosol dispersion within a tubular reactor. In a continuous 6-second process, the aerosol particles were dried, heated and collected. Evaporation of DMF during drying enriched the particles in nonvolatile species of PS-P4VP and carbohydrates, inducing PS-P4VP microphase separation and successive co-assembly and formation PS and P4VP/carbohydrates confined to solid spherical aerosol particle. Heat treatment in argon at high temperature led to direct formation of spherical carbon particles. The aerosol generator (TSI Inc) produced spherical particles with a broad particle size from 1 to 10 μm; monodisperse particles can be produced using a vibration orifice aerosol generator (VOAG). Figure 7 shows representative TEM images of carbon particles. Depending on the block copolymers used and carbohydrate concentrations, carbon particles with worm-like, vesicular, hollow structures were attainable. At relatively low concentration of carbohydrates, particles with worm-like mesostructure (Fig. 7a) were prepared using PS-P4VP. Increasing carbohydrate concentration from 3.2 wt % to 7.3 wt % resulted in vesicular particle mesostructure (Fig. 7b). Distinct from related bulk[33] and thin film[34] lamellar structures that collapse on calcination, the three-dimensional connectivity of the nested spherical shells comprising the vesicular mesophase mechanically stabilizes the structure against collapse during polymer removal. Hollow carbon particles were prepared when PS-PEO was used (Fig. 7c).

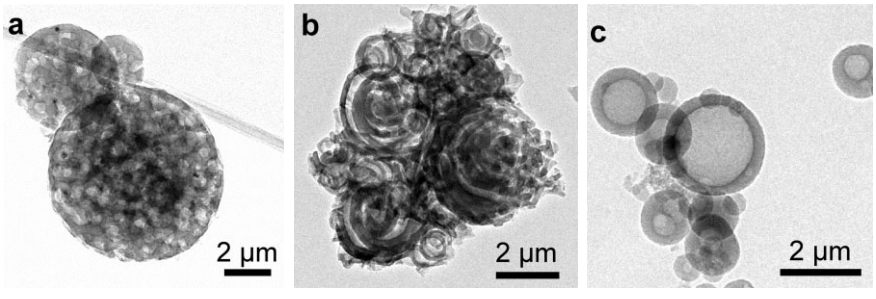

Figure 7. Representative TEM images of nanoporous carbon particles. a) Nanoporous carbon particles were prepared using 3.2 wt % turanose and 1.6 wt % PS-P4VP(polymer source, M_n^{PS} = 12 000 g mol^{-1}, M_n^{PVP} = 11 800 g mol^{-1}, with molecular size distribution of 1.04), showing a uniform pore size of ~27 nm. Sample b was prepared using 7.3 wt % turanose and 1.6 wt % PS-P4VP. Sample c was prepared using 0.2 g turanose and PS-PEO (polymer source, M_n^{PS} = 19 000 g mol^{-1}, M_n^{PEO} = 12 300 g mol^{-1}, with molecular size distribution of 1.04).

3. Conclusions

The hydrogen bonding assisted self-assembly described here, and its elaboration in two different fabrication processes, is a general and direct method to synthesize nanostructured carbon materials. The method is simple and flexible, controlling material form (films and particles), nanostructure, and surface chemistry. The resulting nanostructured carbon materials with 3-dimensional accessible mesoporosity and controlled surface chemistry are of great interest for sensors, sorption and separation, catalysis, control release etc. The method also holds great promise for synthesis of hierarchical organized complex carbon materials by combining the self-assembling solution with other techniques such as soft lithography,[35] photolithography,[36] and rapid printing techniques.[21,37] Through aromatic carbon precursors and higher carbonization temperature, more work is underway to synthesize carbon nanostructures with graphitic microstructures.[38] In addition to the synthesis of carbon materials, we believe that through hydrogen bonding self-assembly between block copolymers with optically, electrically, and magnetically active building blocks such as hydrophilic nanocrystals,[39–41] porphyrins,[42] etc., nanocomposite films, tubes, and particles with precisely positioned nanocrystal and porphyrin units equipped with new optical, electrical, magnetic, and catalytic properties are possible.

4. Experimental

Synthesis of Nanoporous Carbon Films: 0.1 g of PS-P4VP (M_n^{PS} = 12 000 g mol^{-1}, M_n^{PS} = 11 800 g mol^{-1} with molecular size distribution of 1.04, Polymer Source Inc.) was added into 2 g DMF followed by addition of desired amount (3–10 wt %) of carbohydrate precursors, including turanose, raffinose, pentose, glucose, sucrose, etc. The solution was sonicated for 30–60 min to form a homogeneous solution. The samples are then cast or spin-coated onto substrates (silicon wafer, glass slides, gold electrodes, etc.) at 1000 rpm for 2 min. The films were allowed to dry in the fume hood and then placed in a sealed chamber in the presence of solvent vapor such as DMF and benzene, DMF/THF, and DMF/DMSO, etc. for 24 h. The samples were removed and carbonized in an argon environment at 460 °C or higher for 1 h using a heating rate of 1 °C min^{-1}. To enhance hydrogen bonding, the coating solution was heated to 180 °C for 3 h in an autoclave. After natural cooling to room temperature, the solution was used to spin-coat films.

Synthesis of Nanoporous Carbon Particles: 0.1 g of PS-P4VP (M_n^{PS} = 12 000 g mol^{-1},

$M_n^{PS} = 11\,800$ g mol^{-1} or PS-PEO (polymer source, $M_n^{PS} = 19\,000$ g mol^{-1}, $M_n^{PEO} = 12\,300$ g mol^{-1}, with molecular size distribution of 1.04) was added into 6 g DMF followed by addition of 0.1 to 1 g of turanose. The solution was sonicated for 30–60 min to form a homogeneous solution. The solution was then heated at 180 °C for 3 h in an autoclave to form homogeneous dark solution. Spherical carbon particles were prepared using an aerosol reactor (Supporting Information Fig. S8) operated at a volumetric flow rate of 2.6 L STP min^{-1}. Under these conditions, the flow is laminar (Reynolds number at 400 °C, 75) and the entrained aerosol particles experience ~3 s of drying at nominally room temperature followed by ~3 s of heating at 400–500 °C and finally collection on a filter maintained at ~80 °C. Carbonization was conducted in argon at 600 °C for 1 h to create nanoporous carbon particles.

Characterization: SEM images were taken using Hitachi 5200 FEG microscope. TEM was performed on a JEOL 2010 with 200 kV acceleration voltage, equipped with a Gatan slow scan CCD camera. A surface acoustic wave (SAW) technique was used to characterize nitrogen sorption isotherms of mesoporous thin film samples. The samples of thin film for SAW measurement were deposited onto ST-cut quartz SAW substrates followed by carbonization as described above. The SAW devices (97 MHz) on ST-quartz with Ti-primed Au transducers were designed and fabricated at Sandia National Laboratories. In a typical acoustic wave device, an alternating voltage applied to an interdigital transducer on a piezoelectric substrate generates an alternating strain, which launches an acoustic wave. An ASAP 2010 instrument was combined with the SAW device to control the relative pressure; while the SAW device was used to determine the frequency. Mass change was monitored (~80 pg cm^{-2} sensitivity) as a function of relative pressure, assuming that the SAW frequency is only perturbed by a mass loading variation. The GISAXS experiments were performed at the dedicated GISAXS beamline 8-ID-E at the Advanced Photon Source, Argonne National Laboratory. The operating wavelength was 1.66 Å. Images were recorded using a two-dimensional MAR-165 CCD camera with a frame size of 2048 × 2048 pixels (each pixel is 79 μm) mounted behind a vacuum flight path. The sample to detector distance was set to be 1.97 m. The sample sits on a horizontal stage in a vacuum chamber. The sample stage has high precision *x*–*y*–*z* and multiple-rotation motions and is equipped with in-situ heating and cooling elements.

Received: October 13, 2006
Revised: February 24, 2007
Published online: August 31, 2007

[1] P. M. Ajayan, O. Z. Zhou, *Carbon Nanotubes* **2001**, *80*, 391.
[2] H. J. Dai, *Acc. Chem. Res.* **2002**, *35*, 1035.
[3] M. B. Shiflett, H. C. Foley, *Science* **1999**, *285*, 1902.
[4] V. Budarin, J. H. Clark, J. E. Hardy, R. Luque, K. Milkowski, S. J. Tavener, A. J. Wilson, *Angew. Chem. Int. Ed.* **2006**, *45*, 1.
[5] X. M. Sun, Y. D. Li, *Angew. Chem. Int. Ed.* **2004**, *43*, 597.
[6] J. Lee, S. Han, T. Hyeon, *J. Mater. Chem.* **2004**, *14*, 478.
[7] R. Ryoo, S. H. Joo, M. Kruk, M. Jaroniec, *Adv. Mater.* **2001**, *13*, 677.
[8] M. P. Anantram, F. Leonard, *Rep. Prog. Phys.* **2006**, *69*, 507.
[9] J. Kong, N. R. Franklin, C. W. Zhou, M. G. Chapline, S. Peng, K. J. Cho, H. J. Dai, *Science* **2000**, *287*, 622.
[10] S. Yoon, J. W. Lee, T. Hyeon, S. M. Oh, *J. Electrochem. Soc.* **2000**, *147*, 2507.
[11] R. H. Baughman, A. A. Zakhidov, W. A. de Heer, *Science* **2002**, *297*, 787.
[12] Y. Meng, D. Gu, F. Zhang, Y. Shi, H. Yang, Z. Li, C. Yu, B. Tu, D. Y. Zhao, *Angew. Chem. Int. Ed.* **2005**, *44*, 7053.
[13] Y. Meng, D. Gu, F. Zhang, Y. Shi, C. Liang, D. Feng, Z. Wu, Z. Chen, Y. Wan, A. Stein, D. Y. Zhao, *Chem. Mater.* **2006**, *18*, 4447.
[14] G. L. Che, B. B. Lakshmi, E. R. Fisher, C. R. Martin, *Nature* **1998**, *393*, 346.
[15] L. J. Zhi, T. Gorelik, J. S. Wu, U. Kolb, K. Mullen, *J. Am. Chem. Soc.* **2005**, *127*, 12 792.
[16] C. Liang, S. Dai, *J. Am. Chem. Soc.* **2006**, *128*, 5316.
[17] H. Kosonen, S. Valkama, A. Nykanen, M. Toivanen, G. ten Brinke, J. Ruokolainen, I. Ikkala, *Adv. Mater.* **2006**, *18*, 201.
[18] S. Tanaka, N. Nishiyama, Y. Egashira, K. Ueyama, *Chem. Commun.* **2005**, 2125.
[19] C. D. Liang, K. L. Hong, G. A. Guiochon, J. W. Mays, S. Dai, *Angew. Chem. Int. Ed.* **2004**, *43*, 5785.
[20] A. T. Rodriguez, M. Chen, Z. Chen, C. J. Brinker, H. Y. Fan, *J. Am. Chem. Soc.* **2006**, *128*, 9276.
[21] H. Y. Fan, Y. F. Lu, A. Stump, S. T. Reed, T. Baer, R. Schunk, V. PerezLuna, G. P. Lopez, C. J. Brinker, *Nature* **2000**, *405*, 56.
[22] Y. F. Lu, H. Y. Fan, A. Stump, T. L. Ward, T. Rieker, C. J. Brinker, *Nature* **1999**, *398*, 223.
[23] A. Sidorenko, I. Tokarev, S. Minko, M. Stamm, *J. Am. Chem. Soc.* **2003**, *125*, 12 211.
[24] J. Ruokolainen, G. tenBrinke, O. Ikkala, M. Torkkeli, R. Serimaa, *Macromolecules* **1996**, *29*, 3409.
[25] L. C. Cesteros, J. R. Isasi, I. Katime, *Macromolecules* **1993**, *26*, 7256.
[26] Y. X. Wang, S. H. Tan, D. L. Jiang, X. Y. Zhang, *Carbon* **2003**, *41*, 2065.
[27] J. Kim, J. E. Lee, J. Lee, J. H. Yu, B. C. Kim, K. An, Y. Hwang, C. H. Shin, J. G. Park, J. Kim, T. Hyeon, *J. Am. Chem. Soc.* **2006**, *128*, 688.
[28] W. Ruland, B. Smarsly, *J. Appl. Crystallogr.* **2002**, *35*, 624.
[29] K. K. Tenneti, X. F. Chen, C. Y. Li, Y. F. Tu, X. H. Wan, Q. F. Zhou, I. Sics, B. S. Hsiao, *J. Am. Chem. Soc.* **2005**, *127*, 15 481.
[30] G. C. Frye, S. J. Martin, A. J. Ricco, C. J. Brinker, *ACS Symp. Ser.* **1989**, *403*, 208.
[31] H. S. Zhou, S. M. Zhu, M. Hibino, I. Honma, *J. Power Sources* **2003**, *122*, 219.
[32] C. Arbizzani, M. Mastragostino, F. Soavi, *J. Power Sources* **2001**, *100*, 164.
[33] J. S. Beck, J. C. Vartuli, W. J. Roth, M. E. Leonowicz, C. T. Kresge, K. D. Schmitt, C. T. W. Chu, D. H. Olson, E. W. Sheppard, S. B. McCullen, J. B. Higgins, J. L. Schlenker, *J. Am. Chem. Soc.* **1992**, *114*, 10 834.
[34] M. Ogawa, *J. Am. Chem. Soc.* **1994**, *116*, 7941.
[35] P. D. Yang, T. Deng, D. Y. Zhao, P. Y. Feng, D. Pine, B. F. Chmelka, G. M. Whitesides, G. D. Stucky, *Science* **1998**, *282*, 2244.
[36] D. A. Doshi, N. K. Huesing, M. C. Lu, H. Y. Fan, Y. F. Lu, K. Simmons-Potter, B. G. Potter, A. J. Hurd, C. J. Brinker, *Science* **2000**, *290*, 107.
[37] H. Y. Fan, S. Reed, T. Baer, R. Schunk, G. P. Lopez, C. J. Brinker, *Microporous Mesoporous Mater.* **2001**, *44*, 625.
[38] L. J. Zhi, J. S. Wu, J. X. Li, U. Kolb, K. Mullen, *Angew. Chem. Int. Ed.* **2005**, *44*, 2120.
[39] Y. Lin, A. Boker, J. B. He, K. Sill, H. Q. Xiang, C. Abetz, X. F. Li, J. Wang, T. Emrick, S. Long, Q. Wang, A. Balazs, T. P. Russell, *Nature* **2005**, *434*, 55.
[40] H. Y. Fan, K. Yang, D. M. Boye, T. Sigmon, K. J. Malloy, H. F. Xu, G. P. Lopez, C. J. Brinker, *Science* **2004**, *304*, 567.
[41] H. Y. Fan, E. W. Leve, C. Scullin, J. Gabaldon, D. Tallant, S. Bunge, T. Boyle, M. C. Wilson, C. J. Brinker, *Nano Lett.* **2005**, *5(4)*, 645.
[42] J. S. Hu, Y. G. Guo, H. P. Liang, L. J. Wan, L. Jiang, *J. Am. Chem. Soc.* **2005**, *127*, 17 090.